communications biology

A Nature Portfolio journal

Article

https://doi.org/10.1038/s42003-025-07745-1

Early life brain network connectivity antecedents of executive function in children born preterm

Check for updates

Abiot Y. Derbie[1], Mekibib Altaye[2,3], Junqi Wang[4], Armin Allahverdy[1], Lili He[4,5], Leanne Tamm[2,3] & Nehal A. Parikh[1,2,3]

Preterm birth is associated with an increased risk of executive function (EF) deficits, yet the underlying neural mechanisms remain unclear. We combine diffusion MRI, resting-state functional MRI, and graph theory analyses to examine how structural (SC) and functional connectivity (FC) at term-equivalent age (TEA) influence EF outcomes at 3 years corrected age in children born at or below 32 weeks' gestation. Here we show shorter average path length (a measure of efficient structural communication) in the insula is linked to better EF performance, implying that more direct structural pathways in this region facilitate critical cognitive processes. Additionally, higher betweenness centrality (a node-level metric of information flow) in parietal and superior temporal regions is associated with improved EF, reflecting these areas' prominent integrative roles in the whole-brain functional network. Importantly, our multimodal analyses reveal that regional structural efficiency helps shape functional organization, indicating a specific interplay between white-matter architecture and emergent functional hubs at TEA. These findings extend current knowledge by demonstrating how earlier disruptions in SC can alter subsequent FC patterns that support EF. By focusing on precise node-level metrics rather than broad within-network effects, our results clarify the contribution that SC has in guiding functional relationships essential for EF.

Preterm birth is inextricably linked with an increased risk for brain injuries and delayed cerebral maturation, markedly heightening susceptibility to a diverse spectrum of neurodevelopmental disorders and neurocognitive outcomes throughout the individual's lifespan. Despite improved survival rates of preterminfants[1,2], long-lasting neurocognitive sequelae remain the most common concerns faced by children born preterm. Executive functioning (EF) deficits among individuals born preterm can persist well beyond childhood, extending into adolescence and adulthood, underscoring the need to clarify the early neural underpinnings of EF development. EF encompasses working memory, inhibitory control, and cognitive flexibility[3–9], with prevalence estimates ranging from 15% to 50% depending on the specific EF domain and the degree of prematurity[8,10,11]. The successful coordination of EF is contingent upon the architectural robustness and interconnectedness of cortical and subcortical sub-systems, with an essential role for white matter (WM) scaffolding[12–14]. Previous, unimodal structural and functional magnetic resonance imaging (MRI) investigations have elucidated distinct deviations in overall cerebral efficiency and the neural networks underpinning EF deficits in preterm infants compared with term-born controls[3,6,12]. However, the complex interplay between structural and functional brain connectivity, as measured by multimodal MRI, and its contribution to EF development remains underexplored.

Three major forms of brain injury that predict cognitive and EF outcomes in preterm infants are intraventricular hemorrhage (IVH), cystic periventricular leukomalacia (PVL), and diffuse WM abnormality (a milder non-cystic form of PVL)[15–20]. In addition to WM connections, IVH and PVL are often associated with damage to key brain structures including the caudate, thalamus, anterior cingulate cortex (aCG), insula, and posterior parietal cortex [20–23]. These injuries often lead to deficits in EF[7,9,13,20,24,25]. Preterm birth also impacts overall brain development and maturation. Compared to term-born controls, PT infants exhibit alterations in brain structure, including changes in WM connectivity[26,27], reductions in total WM and GM volume[23,28], and decreased cortical surface area, thickness, and

[1]Neurodevelopmental Disorders Prevention Center, Perinatal Institute, Cincinnati Children's Hospital Medical Center, Cincinnati, OH, USA. [2]Department of Pediatrics, Cincinnati Children's Hospital Medical Center, Cincinnati, OH, USA. [3]Department of Pediatrics, University of Cincinnati College of Medicine, Cincinnati, OH, USA. [4]Department of Radiology, Imaging Research Center, Cincinnati Children's Hospital Medical Center, Cincinnati, OH, USA. [5]Department of Radiology, University of Cincinnati College of Medicine, Cincinnati, OH, USA. e-mail: nehal.parikh@cchmc.org

folding[29–31]. Moreover, preterm birth disrupts crucial third-trimester dendritic arborization and synaptogenesis, particularly in prefrontal and parietal association cortices[32,33]. Additionally, major WM tracts are susceptible to injury[22,34], due to the abundance of pre-myelinating oligodendrocytes in the preterm brain[35,36]. This damage alters brain network efficiency by disrupting WM connectivity[34]. These combined GM and WM disturbances profoundly disrupt frontal-subcortical and frontoparietal circuits critical for EF[24,25,37,38]. However, the nature and severity of EF deficits is highly heterogeneous across infants born PT. While there are studies on structural and FC in preterm infants, evidence specifically linking these connectivity measures to EF development at this early age remains limited.

The late third trimester (32–40 weeks' gestational age (GA)) is a critical period for brain network development. This period is characterized by significant growth in WM architecture and a transition from localized connectivity to more integrated networks[39,40]. Although interhemispheric connections emerge relatively early, large-scale networks such as the default mode network (DMN) continue to mature beyond this period, with posterior-anterior connections between key DMN hubs establishing later[41]. Other rudimentary forms of resting-state networks (RSN), including the salience network (SN), central-executive control network (ECN), and dorsal attention network (DAN), also begin to form in late gestation around 30 weeks' GA[40]. These highly organized rich-club networks are particularly susceptible to injury from preterm birth[24,37,40,42,43], and are linked to the cognitive and behavioral challenges frequently observed in preterm children[4,37].

The integrity of distributed functional nodes within the brain's RSN is underpinned by the myelinated WM tracts that enable intricate feed-forward and feed-backward mechanisms fundamental for optimal cognitive function[44,45]. Despite the acknowledged prevalence of structural and functional brain alterations in preterm birth, few studies have examined how these alterations collectively contribute to EF development. Here, we address this gap by investigating how early structural and FC at term-equivalent age (TEA) relate to EF performance at 3 years of age in preterm-born children. Using advanced methods like diffusion MRI (dMRI) and resting-state fMRI (rs-fMRI), we first examine how structural and FC patterns independently associate with EF development. As a secondary, exploratory aim, we investigate potential relationships between structural and FC patterns. We hypothesized that in preterm infants born at or before 32 weeks GA, both SC and FC of key brain regions at TEA would be independently associated with EF outcomes at 3 years, a developmental period when EF becomes more differentiated and reliably measurable. This multimodal approach may offer insights into early brain organization in preterm infants, laying the groundwork for future research into neurodevelopmental processes following preterm birth.

In this study, we demonstrate that structural and functional connectivity at TEA in preterm infants, particularly involving the insula, parietal lobe, and middle superior temporal gyrus, are key determinants of EF outcomes at three years of age. Structurally, shorter average path length in these regions may reflect more efficient white-matter pathways that compensate for early disruptions, thereby supporting foundational EF processes. Functionally, higher betweenness centrality in similar areas could indicate adaptive recruitment of alternative network hubs to maintain cognitive function. These findings suggest that early connectivity patterns can serve compensatory roles for disrupted development and are predictive of later EF performance. Future longitudinal imaging will clarify whether these connectivity profiles remain stable, regress, or specialize over time, ultimately informing how early neural markers might guide interventions to improve cognitive outcomes in children born preterm.

Results

SC and FC modes of inter-subject covariation and sample characteristics

SC and FC modes of inter-subject covariation were extracted using NMF from 358 and 363 participants, respectively. However, for subsequent analyses (including canonical correlation analysis, CCA), the sample was restricted to 212 participants (51.9% female) who had complete data for SC modes, FC modes, and Minnesota Executive Function Scale (MEFS) scores. Baseline characteristics for these 212 participants are reported in Table 1. For comparison, Table 1 also shows the characteristics of the original sample of 363 infants. At the 3-year CA visit, the mean MEFS standard score was 93.1 (SD = 11.9).

Regression model results

The NMF analysis, followed by LASSO feature selection and robust regression, revealed that some of the modes of inter-subject covariation (ISCs) were significantly associated with EF performance. These ISCs predominantly included brain regions such as the insula, middle superior temporal gyrus (mSTG), frontal lobe, and parahippocampal gyrus (PHG). The graph theory metrics that contributed most to these significant ISCs were ASP, cost, and RD.

ISCs from SC analysis included regions spanning diverse cortical and subcortical areas. Key components included the right insula characterized by ASP, the posterior cingulate gyrus and medial superior temporal gyrus white matter (mSTG bilaterally), both characterized by ASP, as well as the frontal lobe (FL) and its white matter showing ASP and cost metrics. Additional components involved regions associated with sensorimotor and cognitive processing, including the anterior middle/inferior temporal gyrus (aM/ITG) with ASP, parietal lobe (PL) and its white matter showing both ASP and cost metrics, and the occipital lobe white matter (OL) demonstrating cost metrics. The cerebellum was also identified with ASP metrics. These components represent both significant and non-significant associations with EF, providing a comprehensive view of structural organization before examining their relationships with EF outcomes.

Table 1 | Maternal and infant clinical characteristics

Baseline variables[a]	Sample with complete data (n = 212)	Original sample with MRI data (N = 363)
Maternal age, M (SD)	29.8 (5.6)	29.2 (5.5)
Maternal smoking during pregnancy	27 (12.7%)	45 (12.4%)
Hypertensive disorders of pregnancy	91 (42.9%)	155 (42.7%)
On mom's own milk at NICU discharge	116 (54.7%)	192 (52.9%)
High social risk	34 (16%)	65 (17.9%)
Antenatal corticosteroids	198 (93.4%)	335 (92.3%)
Female sex	110 (51.9%)	192 (52.9%)
Gestational age, weeks, mean (SD)	29.3 (2.5)	29.3 (2.5)
Birth weight Z-score, mean (SD)	0.075 (1.04)	0.08 (0.99)
Retinopathy of prematurity	68 (32.1%)	122 (33.6%)
Bronchopulmonary dysplasia[†]	82 (38.8%)	149 (41%)
Blood stream infection during hospitalization	20 (9.4%)	40 (11%)
Moderate-severe histologic chorioamnionitis	36 (17%)	53 (14.6%)
Apgar score at 5 min below 5[b]	26 (12.4%)	46 (12.8%)
Postmenstrual age at MRI scan, weeks, mean (SD)	42.8 (1.3)	42.7 (1.4)
Global brain abnormality score, median (IQR)[#]	4 (2, 7)	5 (2, 8)

The comparsion between the sample with complete data (n = 212) and orginal data (N = 363) for both superscript symbols "†" and "#" were not significant ($p > 0.05$).

[a]These clinical and conventional MRI variables were selected a priori for the robust regression model.

[b]Calculated out of 210 as two preterm infants were delivered at home.

Table 2 | Results of the robust linear regression for structural modes of inter-subject covariation (ISCs) derived from diffusion MRI in relation to executive function (EF) at 3 years corrected age in preterm infants

Predictors (ISCs)	Coef.	Coef. 95% CI [LL, UL]	*t*	*p*-value
ISC ASP7	0.136	[−0.68, 0.95]	0.328	0.743
ISC ASP10	−0.022	[−0.82, 0.77]	−0.055	0.956
ISC ASP23	−1.192	[−1.96, −0.43]	−3.059	0.003*
ISC BC20	0.602	[−0.16, 1.36]	1.549	0.121
ISC CC16	0.301	[−0.60, 1.20]	0.655	0.512
ISC CC22	0.605	[−0.19, 1.40]	1.497	0.134
ISC LE6	0.021	[−0.92, 0.96]	0.045	0.964
ISC CC23	0.434	[−0.39, 1.26]	1.036	0.300
ISC CO6	0.787	[0.01, 1.57]	1.977	0.049*
ISC CO28	1.173	[0.36, 1.99]	2.811	0.005*
ISC RD3	−1.087	[−1.95, −0.23]	−2.473	0.014*
ISC RD17	−0.297	[−1.11, 0.52]	−0.713	0.476

Coefficients (Coef.) and 95% confidence intervals ([LL, UL]) are derived from a robust linear model in which only the ISCs that survived the LASSO selection were included. This model controlled for antenatal corticosteroids, gestational age, retinopathy of prematurity, bronchopulmonary dysplasia, high social risk, postmenstrual age at MRI scan, global brain abnormality score, maternal age, hypertensive disorders of pregnancy, moderate-severe histologic chorioamnionitis, maternal smoking, Apgar score at 5 min below 5, bloodstream infection, and receiving mother's own milk at NICU discharge. Covariates were standardized, and heteroskedasticity-consistent standard errors were used. A single asterisk (*) indicates $p < 0.05$.
ISCs modes of inter-subject covariation, *ASP* average path length, *BC* betweenness centrality, *CC* clustering coefficient, *LE* local efficiency, *CO* cost, *RD* regional degree

Table 3 | Results of the robust linear regression for functional modes of inter-subject covariation (ISCs) derived from resting-state fMRI in relation to executive function (EF) at 3 years corrected age in preterm infants

Predictors (ISCs)	Coef.	Coef. 95% CI [LL, UL]	t	*p*-value
ISC ASP8	−0.693	[−2.89, 1.50]	−0.620	0.536
ISC ASP19	−0.008	[−0.84, 0.83]	−0.020	0.984
ISC BC4	−0.737	[−1.65, 0.18]	−1.582	0.115
ISC BC5	0.819	[−0.06, 1.70]	1.834	0.068
ISC BC15	1.422	[0.57, 2.27]	3.273	0.001*
ISC BC23	0.559	[−0.29, 1.40]	1.298	0.196
ISC CC20	0.249	[−0.83, 1.33]	0.450	0.653
ISC CC22	−0.447	[−2.57, 1.67]	−0.413	0.680
ISC CO6	0.833	[−0.08, 1.75]	1.783	0.076
ISC CO27	1.160	[0.26, 2.06]	2.534	0.012*
ISC LE6	0.261	[−0.72, 1.24]	0.522	0.602
ISC LE7	−0.844	[−1.81, 0.12]	−1.717	0.088
ISC LE8	−0.917	[−1.82, −0.01]	−1.985	0.049*
ISC LE12	0.513	[−0.39, 1.42]	1.109	0.269
ISC LE15	−0.490	[−1.35, 0.37]	−1.122	0.263
ISC LE16	−0.376	[−1.44, 0.68]	−0.696	0.488

Coefficients (Coef.) and 95% confidence intervals ([LL, UL]) are derived from a robust linear model in which only the ISCs that survived the LASSO selection were included. This model controlled for antenatal corticosteroids, gestational age, retinopathy of prematurity, bronchopulmonary dysplasia, high social risk, postmenstrual age at MRI scan, global brain abnormality score, maternal age, hypertensive disorders of pregnancy, moderate-severe histologic chorioamnionitis, maternal smoking, Apgar score at 5 min below 5, blood stream infection, and receiving mother's own milk at NICU discharge. Covariates were standardized, and heteroskedasticity-consistent standard errors were used. A single asterisk (*) indicates $p < 0.05$.
ISCs modes of inter-subject covariation, *ASP* average path length, *BC* betweenness centrality, *CC* clustering coefficient, *CO* cost, *LE* local efficiency.

The robust regression analysis using dMRI metrics (Table 2) revealed there was a significant negative correlation between the ASP (ISC 23) and the MEFS score ($\beta = -1.19$, $p = 0.002$). ISC 23 featured bilateral insular regions as its primary contributors. Additionally, a higher cost graph theory metric within ISC CO6 and ISC CO28 was positively associated with improved EF performance ($\beta = 0.79$, $p < 0.05$ and $\beta = 1.17$, $p < 0.01$, respectively). The aPHG and the FL demonstrated the highest cost within those two ISCs. Last, the regional degree metric, reflecting the number of direct connections a brain region has within the network, indicated that ISC RD3, dominated by the right OL, FL, and PL, showed a negative association with EF performance ($\beta = -1.09$, SE = 0.440, $p < 0.05$).

ISCs derived from FC analysis encompassed regions spanning a range of cognitive and sensory pathways. Within these, the anterior lateral temporal lobe white matter (aLTL) and aCG were characterized by BC, and the medial superior temporal gyrus (mSTG) showing cost metrics. Components relevant to visual and cognitive processing included the lateral occipito-temporal gyrus/anterior fusiform gyrus (LOTG/aFuG) with BC, and OL showing cost metrics in both gray and white matter. The pM/ITG demonstrated BC, while its gray matter showed bilateral cost metrics. Additional regions involved memory and cognitive processing, such as the hippocampus showing local efficiency, pPHG and caudate with cost metrics, and parietal lobe (PL) demonstrating local efficiency. The frontal lobe (FL) showed cost metrics. These components represent both significant and non-significant associations with EF, providing a comprehensive view of functional organization in our cohort before examining their relationships with EF outcomes.

The robust regression analysis using rs-fMRI metrics (Table 3) revealed that ISC 15 of the BC graph metric was directly associated with EF ($\beta = 1.42$ SE = 0.434, $p < 0.01$). ISC 15 was notable for higher betweenness centrality in posterior parietal regions. Furthermore, ISC 27 of the cost graph metric demonstrated a significant direct association with EF ($\beta = 1.16$, $p < 0.05$), exhibiting high-cost values in occipital and frontal areas. Additionally, the analysis identified ISC 8 of the LE graph theory metric as another significant contributor to EF. The LE graph theory metric of ISC 8 was inversely associated with EF ($\beta = -0.92$, SE = 0.462, $p < 0.05$), with the right pSTG WM as the highest-contributing region.

Our primary findings focus on these ISCs derived from NMF and their associations with EF. Additional exploratory analyses investigating structure–function relationships are presented in Supplementary Information. The CCA revealed two significant canonical pairs (Fig. 1a, b). First, structural features within temporal and frontal lobes were associated with functional characteristics in occipital and medial temporal areas ($R^2 = 0.25$, pFDR < 0.001), suggesting that structural efficiency of these regions shapes their functional organization. Second, SC in superior temporal, parietal, and frontal lobes was associated with FC in medial temporal and occipital lobes ($R^2 = 0.14$, pFDR < 0.05), highlighting the role of structural attributes in supporting functional networks. Additionally, by weighting their canonical coefficients, we further examined the associations of each SC and FC covariate (Fig. 2a, b). The analysis revealed that structural graph theory metrics of ASP in the cerebellum, PL, mSTG, insula, and FL were each associated to cost and LE graph theory metrics of the FC in OL, posterior parahippocampal gyrus (pPHG), caudate and hippocampus. Full details of these canonical pairs and their implications are provided in supplementary information.

Discussion

This is the first study in preterm infants to investigate the early development of structural and functional networks at TEA that subserve EF development at 3 years CA. We accomplished this goal by studying a large and diverse cohort of preterm infants recruited from five academic and non-academic NICUs from a geographically defined region of Southwest Ohio. We assessed EF at 3 years of age because it represents a developmentally meaningful time point at which EF skills become more stable and measurable, and the MEFS used in this study is validated for this age group. Our

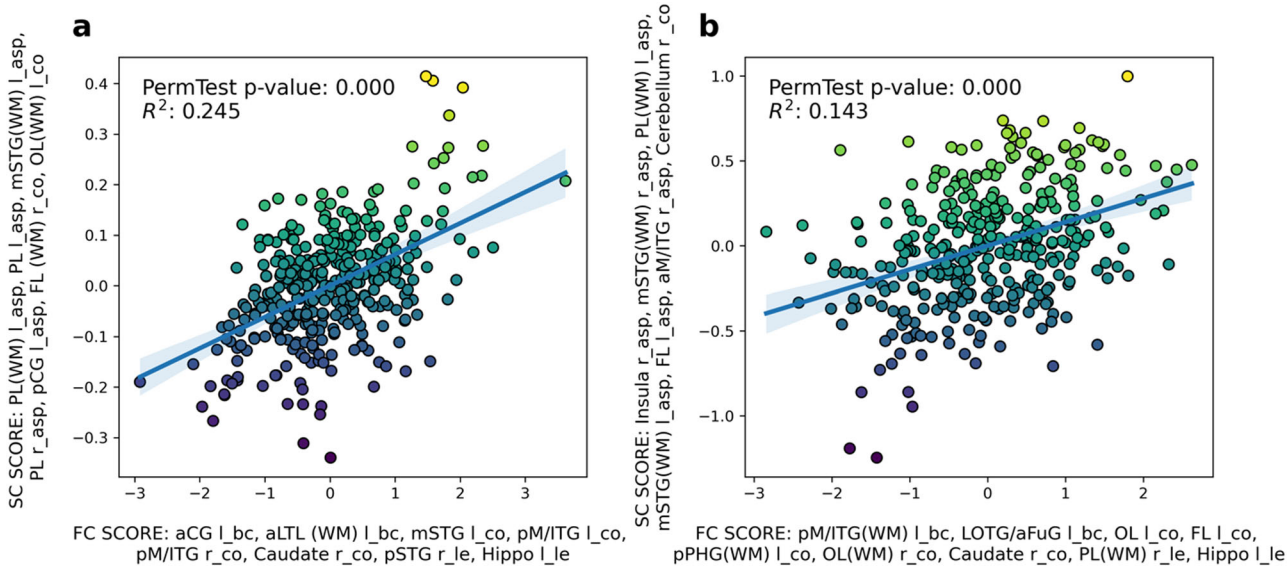

Fig. 1 | Canonical correlation analysis of structural and functional connectivity. Scatter plots represent the associations between transformed SC and FC scores for the two significant canonical covariate pairs. **a** First significant canonical pair demonstrates the association between SC and FC scores with an $R^2 = 0.245$ (FDR corrected $p < 0.001$). **b** Second significant canonical pair show a similar association with an $R^2 = 0.143$ (FDR corrected $p < 0.001$). Each pair shows the relationship between structural connectivity (SC) and functional connectivity (FC) network components. The marker size and opacity within each plot are adjusted to the connectivity scores' strength and *p*-values.

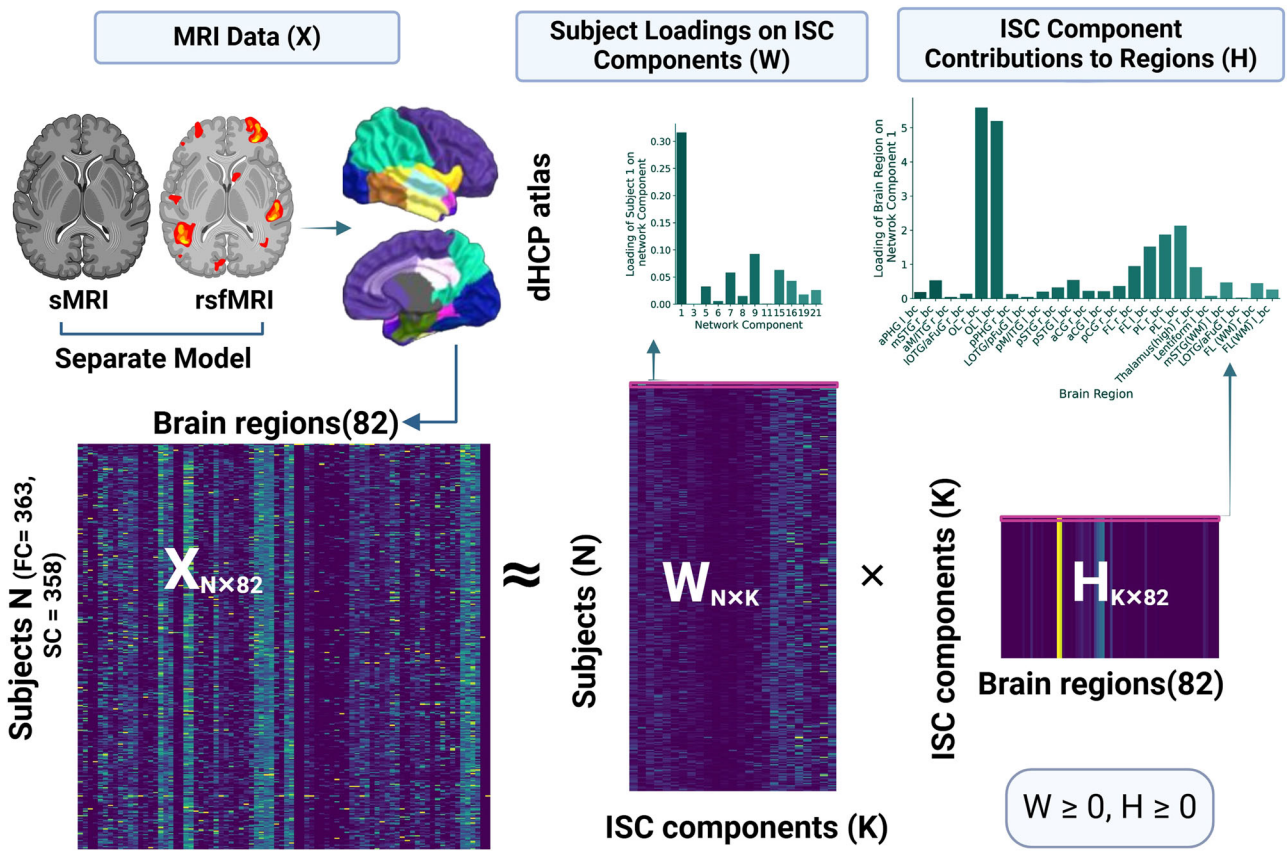

Fig. 2 | Non-negative Matrix Factorization. In this schematic, **X** is the original data matrix comprising rows for subjects (**N**) and columns for brain regions (82). By factorizing **X** into two non-negative matrices, **W** and **H**, NMF identifies modes of inter-subject covariation in the data. The matrix **W** contains subject loadings, indicating how strongly each subject expresses a given mode; the histogram above **W** shows example loadings for one subject across multiple modes. The matrix **H** details the contributions of each brain region to these modes; the histogram above **H** illustrates a row of **H**, enumerating the regions and their respective weights in one mode. Separate NMF models were applied to structural connectivity (SC, N = 358) and functional connectivity (FC, N = 363).

study revealed three key findings: (1) SC in regions such as the insula, middle superior temporal gyrus (mSTG), frontal lobe (FL), and PHG was associated with EF performance; (2) FC in parietal and temporal areas was linked to EF development; and (3) certain structural features appeared to shape functional organization in ways crucial for EF. These observations extend current knowledge by demonstrating how early brain connectivity patterns may influence EF development in preterm infants. For instance, our finding of the insula's involvement in EF aligns with prior research[46] while extending it to the preterm population. Notably, higher connection density in certain frontal and temporal regions positively correlated with EF outcomes, whereas degree metrics in areas linked to attention showed a negative association. In addition, parietal lobe (PL) connectivity measures implicated in information flow were related to EF, highlighting the importance of integrative processing. While these findings provide insights into early markers of EF development, further longitudinal studies are needed before they can inform clinical interventions. Our findings highlight the unique structure–function associations in the preterm brain and suggest a broadly distributed reliance on multiple regions for EF processing. These findings offer insights into the organizational basis of EF in preterm infants, where the SC analyses indicate that certain white matter tracts may scaffold the more distributed functional activities observed in the FC data. Next, we describe each of our three findings in more detail.

With regards to SC and its association with EF, our findings refine the understanding of the associations between SC and EF in preterm infants, demonstrating that the efficiency of information transfer in these interconnected regions is inherently linked to their structural coupling during EF, with the insula and the mSTG playing a key role (ASP ISC23). The study identified positive associations between the cost (density of connections) in ISC CO6 and ISC CO28 and EF performance. Although ISC CO28 and ISC CO6 show overlapping features with well-known higher-order networks, both had high costs in the anterior parahippocampal gyrus and frontal lobe, respectively. The structural efficiency of key regions, such as the insula, mSTG, FL, OL, PHG, and PL, as well as the density, nodal connectivity, and centrality of these structural connections, shape EF in preterm infants. The cost metric for both ISCs CO06 and CO28 highlighted the WM of the FL and PL, integral to attentional and cognitive control and serving as the basis for visuospatial processing[47,48]. The average ASP and cost metric reflect the agility of information transit within the EF circuitry[49] and the metabolic and developmental investments in maintaining these neural pathways[50], respectively. This increased SC may reflect the brain's compensatory mechanisms or adaptive plasticity in response to preterm birth, potentially supporting the development of cognitive control and working memory processes essential for EF. The connectivity patterns of the insula and FL correlate with cognitive control, and the involvement of the right PL underlines attentional mechanisms, thereby contributing to EF maturation in preterminfants[45,51]. We also observed that the regions comprising ISC RD3, specifically the right OL, FL, PL, and thalamic areas, align with the functional domains of visual processing and attention networks, indicative of their role as well-connected neural hubs, with their SC, as quantified by RD and ASP, being associated with emerging cognition in both preterm and term infants[40,52,53]. Moreover, our findings suggest a non-linear relationship between regional connectivity in ISC RD3 and EF, possibly attributable to a disproportionate emphasis on local versus distributed processing[54,55], aligning with the concept of neural efficiency and supporting the notion that specialized regions must effectively relate to enable complex functions[44,56,57], while providing unique insights into the association between structural topology, efficiency, and emerging EF in high-risk preterm infants through the elucidation of RD centrality. In structural analyses, shorter average path length in the insula and parietal regions may reflect efficient white-matter pathways that partly compensate for neonatal disruptions, potentially supporting foundational EF skills.

With regards to FC and EF, our results revealed the BC (reflecting information flow and communication between brain regions) of the left PL's WM (ISC BC5) as a central conduit, showing its role in cognitive processes pivotal to EF such as attentional control and working memory. This finding aligns with existing research identifying the aMTL and PL as core components involved in EF maturation in preterm infants scanned at TEA[42]. The BC of the PL suggests its strategic role as a key hub supporting the view that its intermediacy appears particularly vital for facilitating EFs in preterm children scanned at school age[27,58]. Concurrently, the cost-efficiency metric within ISC CO27 offers a window into the functional significance of the FL and PHG. The density of connections (cost) in these areas, in concert with the OL, is integral to visual and memory-related processing, with a marked left hemispheric dominance that may underlie early cognitive functions. The correlation between the efficiency of ISC CO27 and EF scores shows the nature of efficient neural connectivity for cognitive maturation in preterm infants and aligns with results using longitudinal network analysis in infants scanned from birth to TEA[42], demonstrating that the strength and spatial extent of RSN increased with advancing postmenstrual age, suggesting ongoing network development and maturation. In ISC LE8, the LE metrics substantiate the significance of the left PL and FL, along with the bilateral cerebellum, supporting previous studies of these regions in cognitive development of adolescents and young adults born preterm[12,20]. The negative association between the LE of the pSTG and EF in preterm infants suggests that lower LE of the pSTG results from perinatal brain injury and/or brain immaturity. This finding is consistent with the concept of neural inefficiency, where a less efficient brain requires more resources to perform a given task[57]. Perinatal brain injury and immaturity can lead to disrupted neural connectivity and organization, resulting in reduced LE of specific brain areas, such as the pSTG, as demonstrated in studies of infants and preadolescents born preterm[24,59]. Consequently, there may be advantages to focusing on the development of other positive regional networks to advance EF development. The compensatory mechanism may involve the recruitment of additional brain networks to support EF as the result of inefficient specialized networks, as shown in studies of preterm infants scanned longitudinally from birth to TEA[42,59,60]. Our findings both align with and extend previous studies on older preterm children and adults. For instance, our observation of altered connectivity in higher-order networks is consistent with findings in older preterm populations. However, our study uniquely demonstrates that these alterations are already present at term-equivalent age and are predictive of later EF performance. Conversely, in functional analyses, higher betweenness centrality in these same areas could indicate an adaptive recruitment of alternative network hubs to maintain cognitive function. Whether these patterns remain stable, regress, or further specialize depends on longitudinal developmental trajectories. Future imaging at multiple time points will clarify whether these early connectivity profiles solidify into long-term compensatory mechanisms or eventually give way to more specialized organization as children mature.

The functional–functional associations shown in our analysis underscore how the SN, ECN, and DMN collectively contribute to early EF development in preterm infants. Previous studies in adults have indicated that the DMN is less directly associated with EF, with the ECN and SN being more consistently involved in EF[61,62]. However, our findings suggest that in the context of preterm infants, the DMN may play an even more integral role in the early stages of EF development. This is a pivotal distinction, as it indicates that the preterm brain may utilize the DMN differently or more extensively in supporting the emergence of executive capacities compared to term-born counterparts. Such extended associations across these networks in preterm infants underscore a divergent pattern of neural integration and suggest that these children might engage alternative or additional neural resources to support EF. This view is supported by studies showing that children born preterm engage in atypical language pathways to perform comparably to term peers[59,60]. This adaptability is indicative of the inherent neuroplasticity in the developing preterm brain[63] and highlights the importance of tailored investigations into the unique trajectories of EF maturation in preterm infants. Our findings of distributed network support for EF in preterm infants align with observations in other cognitive domains, such as language development. For instance, Scheinost, et al.[64] reported that preterm infants tend to utilize more right-hemisphere homologs of left-hemisphere language

regions, suggesting a more distributed language network. This parallel between EF and language networks raises the question of whether these distributed patterns represent compensatory mechanisms or deficits. The engagement of broader neural networks could reflect the preterm brain's adaptive plasticity, recruiting additional resources to support cognitive functions. Alternatively, it might indicate a delay in the specialization and segregation of functional networks. Future research combining longitudinal imaging with detailed cognitive assessments could help differentiate between these possibilities. Moreover, this distributed pattern may extend to other cognitive functions in preterm infants, highlighting the importance of considering whole-brain network reorganization when studying neurodevelopmental outcomes in this population.

Our study has three primary limitations. First, EF remains a complex and evolving construct, particularly during early childhood, and no universally validated measure exists for children younger than 3. While the MEFS is among the few tools validated at this age, it captures EF in a unidimensional manner. We are currently collecting more refined EF measures at ages 5 and 7 to build upon these initial findings. Second, interpreting the modes of ISCs from NMF must be done with caution, as they reflect data-driven patterns rather than strictly delineated networks. Third, although our sample is large and diverse, the developmental trajectory of preterm-born children can vary widely, necessitating longitudinal imaging to confirm whether these early connectivity patterns stabilize or evolve over time.

While our findings provide insights into the structural and functional organization of the preterm brain, the immediate translation of these network measures into clinical interventions remains premature. Rather than offering direct clinical guidelines, our results should be viewed as hypothesis-generating, opening avenues for future inquiries into early neurodevelopmental processes. Prospective longitudinal studies and targeted intervention trials will be essential to determine whether the identified connectivity patterns can be leveraged to improve executive outcomes or to develop precision-based interventions tailored to infants at highest risk of EF deficits. This work thus lays an early foundation for understanding the neurobiological underpinnings of EF development in preterm infants, highlighting how specific structural and functional configurations may scaffold emerging cognitive control. Building on our observations, subsequent research could examine whether particular connectivity profiles reliably predict discrete EF subcomponents—such as inhibitory control, cognitive flexibility, or working memory—and whether targeted interventions can reinforce beneficial brain network arrangements. Additionally, these measures might serve as early biomarkers, enabling clinicians to identify infants who would benefit from enhanced monitoring or proactive support. However, significant further investigation, including repeated neuroimaging across multiple time points and randomized interventions, must precede any clinical application of our findings. Despite these limitations, our study has several noteworthy strengths. First, it is the earliest investigation to apply multimodal, advanced graph-theoretical methods (NMF, CCA) to a large sample of preterm infants, controlling for key clinical variables and thus enhancing the validity of our conclusions. Second, we were able to capture brain development near term-equivalent age, before extensive environmental influences could confound the relationship between early brain connectivity and EF outcomes. Although the direct clinical implications remain to be established, our results underscore the importance of continued research into the neural architecture underpinning EF in this vulnerable population.

In conclusion, our results show that structural and FC at TEA—particularly involving the insula, parietal lobe, and middle superior temporal gyrus—are key determinants of EF development at 3 years CA in preterm infants. These infants may rely on a more distributed network architecture for EF processing, perhaps reflecting adaptive mechanisms for developmental disruptions. By considering both local and global changes in structural and FC, our findings deepen the understanding of neurodevelopmental consequences of preterm birth and pave the way for future research on how these early connectivity markers might predict and potentially improve long-term cognitive outcomes.

Methods

Participants

Data for this study came from a large ($n = 395$) prospectively studied cohort that recruited preterm infants born at or below 32 weeks' GA from five Greater Cincinnati area level-III/IV neonatal intensive care units (NICUs) between June 2017 and November 2019. Institutional ethics approval was obtained from the Cincinnati Children's Hospital Medical Center Institutional Review Board, with reciprocal consent from the four additional NICUs. Before enrollment, written informed consent was obtained from each infant's parent or legal guardian. All ethical regulations relevant to human research participants were followed. The original cohort excluded infants with congenital brain malformations, cyanotic heart defects, or chromosomal anomalies. For this sub-study, we excluded infants due to motion-corrupted diffusion MRI ($n = 32$), inability to complete EF assessment ($n = 91$), and not having either rs-fMRI or dMRI data ($n = 60$) from the original sample of 395 infants resulting in a sample size of 212. All participants with MRI data SC: $n = 358$; FC: $n = 363$) were initially considered for deriving the modes of inter-subject covariation (see below). For subsequent analyses linking MRI to EF, 212 participants with complete imaging and EF data were included.

Procedures

All infants underwent an anatomic MRI, rs-fMRI, and dMRI around their expected birthdate. Caregivers completed a demographic survey at study enrollment which included information on six socioeconomic factors: family structure, household income, employment status of primary provider, language spoken at home, maternal age at birth, and education of primary caregiver. This information was utilized to derive a social risk score as per Roberts et al. with one difference – we replaced occupation of primary provider with household income[65] as previously described[66]. Scores ranged from 0 to 12 with higher scores indicating higher social risk; scores of >6 were considered high risk. All clinical data were collected prospectively from maternal and infant electronic medical records by trained clinical research coordinators or nurses using predefined variables. Specifically, clinical characteristics, pregnancy/delivery data, and neonatal intensive care unit (NICU) parameters were systematically recorded following a standardized protocol. The data collection process adhered to rigorous methodologies to ensure accuracy and completeness, mirroring the structured approach used by Parikh et al.[67] to document perinatal risk and protective factors associated with neurodevelopmental outcomes. At 3 years corrected age (CA), a rigorously trained, certified examiner—masked to imaging findings—administered the executive function (EF) assessment to the child on an Android tablet. The assessment protocol followed standardized guidelines to ensure consistency across participants, minimizing potential biases in measurement.

EF assessment

The MEFS is a computerized application based on the Dimensional Change Card Sort Task[68,69], measuring cognitive flexibility, working memory, and inhibitory control. MEFS yields an age-normed standard score ($M = 100$, $SD = 15$) reflecting a unidimensional EF construct in early childhood[70]. We chose to assess EF at 3 years of age as it provides a more stable measure compared to earlier time points like 18 months. At 3 years, EF becomes more differentiated and measurable. The MEFS tasks children to sort cards that progressively increase in complexity with an adaptive algorithm that adjusts the difficulty in real-time based on the child's performance, ensuring an appropriate challenge level. The MEFS demonstrates robust psychometric properties, including high reliability (intraclass correlation coefficient = 0.93), and has been extensively validated in over 7000 children, including those down to 2 years of age[71,72], and is sensitive to age-related EF development[73]. Higher MEFS scores indicate higher EF.

The comprehensive methodological approach employed in this study, combining advanced neuroimaging techniques (dMRI and rs-fMRI) with sophisticated analytical methods (NMF and LASSO), allows for a better exploration of the complex interplay between structural and functional brain connectivity in preterm infants. By examining both structural and functional connectomes, we aim to better understand how early brain organization at TEA relates to later EF development. The use of ISC and their association with EF scores provides a more holistic view of brain network dynamics, moving beyond simple region-to-region connections. This approach, while exploratory in nature, represents a first step in comprehensively investigating the relationship between early brain connectivity patterns and EF in preterm infants. By capturing the intricacies of brain development and function in this group, we hope to lay the groundwork for future research that may inform our understanding of neurodevelopmental processes following preterm birth. It's important to note that as a basic associative study, our findings are preliminary and will require further validation before any clinical applications can be considered.

MRI data acquisition

The use of both structural and functional neuroimaging modalities in our study is crucial for comprehensively understanding brain development and function in preterm infants. This multimodal approach allows us to examine how structural changes may underpin functional adaptations, offering a more complete picture of brain organization in preterm infants.

Infants were scanned on a single 3 T Philips Ingenia MRI scanner (Best, Netherlands) using a 32-channel head coil. Diffusion-weighted imaging (DWI) was performed using b = 800 s/mm². The acquisition parameters were: TE/TR = 88/6972 ms, 90° flip angle, FOV = 160 × 160 mm², resolution=2.0 × 2.0 × 2.0 mm³, no SENSE or multiband factor, 36 directions, 5:58 min acquisition time.

The rs-fMRI data were acquired using the following parameters: TR = 1195 ms, TE = 45 ms, flip angle=55°, resolution=2.5 × 2.5 × 2.5 mm³, multiband factor=3, with 400 frames collected over 8:12 min. High-resolution anatomical scans were obtained using axial T2-weighted (TE/TR = 166/10,000 ms, 90° flip angle, 1.0 × 1.0 × 1.0 mm³ voxels, 3:53 min), sagittal 3D T1-weighted (TE/TR = 3.4/7.3 ms, 11° flip angle, 1.0 × 1.0 × 1.0 mm³ voxels, 2:47 min), and axial susceptibility-weighted imaging (TE/TR = 7.2/29 ms, 17° flip angle, 0.57 × 0.57 × 1.00 mm³ voxels, 3:27 min) sequences.

Structural preprocessing and connectome construction

All diffusion MRI (dMRI) data were preprocessed using the FMRIB Software Library (FSL)[74] to correct for off-resonance field effects, eddy current distortions, and subject motion. Specifically, we first employed FSL's topup to estimate and correct off-resonance fields, followed by FSL's eddy tool with outlier replacement to address eddy current-induced distortions and residual head motion. These steps ensured that potential artifacts were minimized prior to further analyses. Next, each infant's diffusion data were registered to their age-matched anatomical image using a boundary-based registration (BBR) approach and non-linear registration via FNIRT[75,76]. An automated quality control procedure was then applied, discarding volumes with framewise displacements exceeding 0.3 mm or substantial signal dropout. Subsequently, we computed advanced diffusion metrics (fractional anisotropy (FA)), based on a diffusion kurtosis-augmented (DKI) tensor model[77]. To accurately reconstruct fiber pathways, we leveraged the MRtrix3 toolbox[78] and accounted for the unique properties of the neonatal brain. Unlike the adult brain, neonatal white matter exhibits lower anisotropy, posing additional challenges for diffusion modeling. In this study, we employed a traditional tensor-based approach using a single *b*-value ($b = 800$ s/mm²), which remains appropriate for our neonatal sample. Although advanced spherical deconvolution methods can accommodate crossing fibers more flexibly, our acquisition parameters and single-shell design are more suitably analyzed via this standard tensor model. We visually inspected the resulting tractography to ensure alignment and coverage of major white-matter pathways in these preterm infants, yielding robust connectome reconstructions at term-equivalent age. This approach provides more reliable fiber-orientation estimates and, by extension, more accurate connectome construction. For node definition, we employed the developing Human Connectome Project (dHCP) neonatal brain atlas[79,80], which partitions the brain into 82 cortical and subcortical regions of interest (ROIs). Each infant's T2-weighted anatomical scan was non-linearly registered to the dHCP T2-weighted template using Advanced Normalization Tools (ANTs)[81], and this transformation was then applied to the dHCP atlas, bringing the 82 ROIs into the infant's native space. We visually inspected each registration to ensure alignment quality, and subsequently, the diffusion data were registered to the T2-weighted image via a rigid-body transformation[82]. To derive each infant's structural connectome, we computed the mean FA values for all fiber tracts connecting each pair of the 82 ROIs. This yielded a symmetric 82×82 adjacency matrix, where each cell reflects the FA-weighted SC strength between the corresponding ROIs. These matrices thus served as individualized, anatomically informed representations of each infant's early structural brain network.

Functional preprocessing and connectome construction

The rs-fMRI data were preprocessed using the dHCP functional pipeline[83], including distortion correction, slice-to-volume motion correction, and structured noise denoising. Using the same 82-region atlas[84], Pearson correlations between each pair of ROIs were computed, generating an 82×82 adjacency matrix characterizing FC.

Graph theory analysis of structural and functional connectome

Graph theory metrics for both functional and structural brain connectivity were computed using Brain Connectivity Toolbox[85]. We derived the following metrics to enable a detailed characterization of the brain networks: 1) degree (the number of connections linked to a node), 2) cost (the ratio of existing connections to possible connections for a node), 3) betweenness centrality (BC: a measure of a node's centrality in a network, determining its influence over information flow), 4) average path length (ASP: the mean distance between a node and all other nodes), 5) clustering coefficient (CC: indicating the degree to which nodes in a network tend to cluster together), 6) local efficiency (LE: reflecting the efficiency of information transfer in the immediate neighborhood of a node), and 7) global efficiency (GE: a measure of the network's overall efficiency in information transfer). Graph theory values for both the structural and functional connectome are generated for all 82 nodes for each of the graph theory metrics except GE (global brain measure).

Modes of Inter-Subject Covariation (ISC) via Non-negative Matrix Factorization (NMF). We employed non-negative matrix factorization (NMF) to identify modes of inter-subject covariation (ISC) in graph-theoretical metrics derived from both SC and FC[86,87]. Specifically, SC ($N = 358$) and FC ($N = 363$) data were organized into matrices $X \in \mathbb{R}^{N \times 82}$, where each row contained node-level metrics for an individual infant. NMF factorized these matrices into two non-negative matrices, **W** (subject loadings) and **H** (regional contributions), such that $X \approx W \times H$. By enforcing non-negativity, NMF reveals positively valued, overlapping patterns of variability in SC and FC. We evaluated a range of possible mode numbers ($\mathbf{k} = 2$ to 31) and selected the optimal **k** by iteratively adjusting an adaptive relative error threshold, thereby balancing model accuracy with complexity[88,89]. Once the optimal number of modes was determined, NMF was re-initialized and refitted to ensure stable results. Finally, we retained regions exceeding a conservative 1% contribution threshold in **H**, following established guidelines (e.g. Sotiras, et al.[90]), which yielded interpretable modes of inter-subject covariation in the graph metrics (Fig. 3).

The ensuing basis matrices $\mathbf{W}_{sc}$ and $\mathbf{W}_{fc}$, were concatenated to compose an integrated feature set, encapsulating the collective connectivity profile. These composite features were then employed in the least absolute shrinkage and selection operator (LASSO) model.

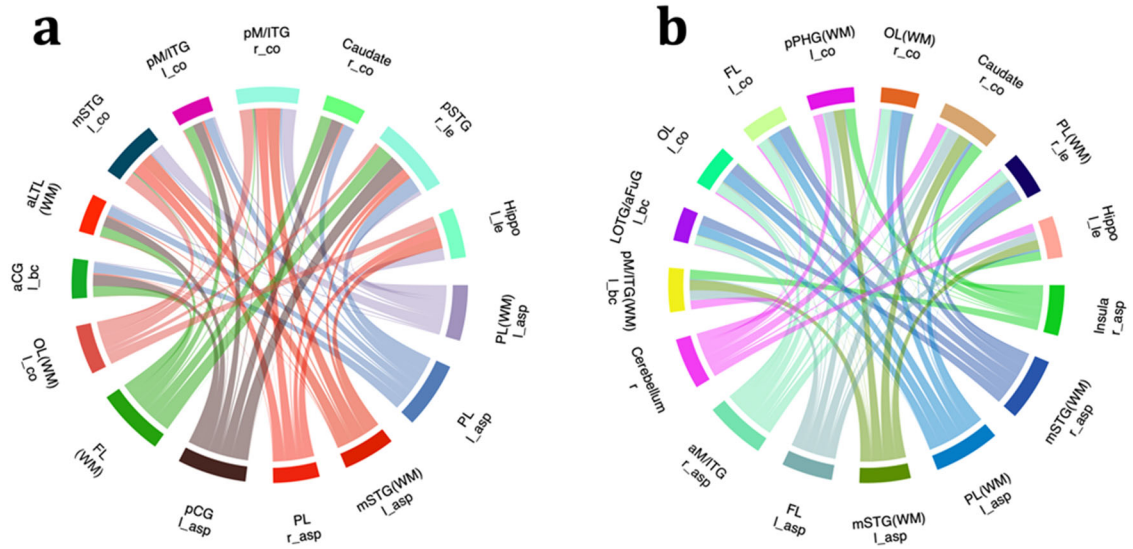

Fig. 3 | Canonical associations between structural and functional connectivity. This multimodal connectivity circos plot for the canonical covariate pairs shows the intricate associations between FC and SC variables across two unique canonical covariate pairs 1 (**a**) and 2 (**b**). The SC variables are depicted along the radial axis, serving as the basis for the inner tracks. Correspondingly, the FC variables are shown as segments along the circular edge. The chords connecting FC and SC variables indicate their mutual influence, quantified by the weighted canonical correlation, and demonstrate the integrated nature of structural and functional attributes in each canonical variate pair. The thickness of each chord is proportional to the combined canonical weights of the connecting variables, serving as a visual proxy for the magnitude of their interaction.

Feature selection and regularization using LASSO

To link these NMF-derived modes to EF, we employed LASSO regression with embedded feature selection. The standard MEFS score served as the outcome, while each individual's loadings on the modes (from **W**) acted as predictors. We used 10-fold cross-validation to identify the alpha parameter that minimized out-of-sample prediction error; the final model was refitted on the entire dataset to obtain predictions and estimate mean squared error. Features surviving LASSO shrinkage are thus considered key candidates in explaining EF variability.

Robust regression models

For final inference, we included only those modes that survived LASSO in a robust linear regression (MASS package in R). The following clinical confounders were controlled for in the regression model: antenatal corticosteroids (ACS), GA, retinopathy of prematurity (ROP), bronchopulmonary dysplasia (BPD)[91], high social risk, postmenstrual age at MRI scan (PMA), global brain abnormality score[92], maternal age (MA), hypertensive disorders of pregnancy (HDP), moderate-severe histologic chorioamnionitis, maternal smoking during pregnancy, Apgar score at 5 min below 5, blood stream infection during hospitalization, and receiving mother's own milk at NICU discharge. Covariates were standardized, and robust standard errors were computed using heteroskedasticity-consistent estimates from the 'sandwich' package[93]. Coefficients represent independent effects of each mode on EF, adjusted for all other variables.

Exploratory Canonical Correlation Analysis (CCA)

As a secondary, exploratory analysis (detailed in the Supplementary Information), we performed CCA to investigate structure–function relationships among NMF-derived modes that were significantly related to EF (Supplementary Figs. 1 and 2). We applied FDR correction for multiple comparisons. This analysis aims to elucidate how structural properties might shape functional organization, rather than re-evaluating EF associations.

Statistics and reproducibility

In this study, a total of 212 preterm infants (≤32 weeks' gestation) were included, each having complete data for dMRI, rs-fMRI, and EF assessments at 3 years CA. Because this investigation focused on how individual-level brain measures relate to EF outcomes, each infant constitutes a unique biological replicate; no technical replicates were undertaken. The final sample size of 212, drawn from an original cohort of 395, was determined by data availability, as infants with missing or motion-corrupted scans were excluded to ensure consistent data quality.

All statistical analyses were conducted using R (version 4.1.0 or later). First, graph-theoretical metrics (including average path length, cost, betweenness centrality, clustering coefficient, local efficiency, and regional degree) were computed for 82 brain regions in both structural and functional connectomes, derived respectively from dMRI and rs-fMRI data. Next, NMF was applied separately to these structural and functional measures to identify ISCs. These ISCs represent data-driven patterns in connectivity, rather than predefined resting-state networks.

To select the most relevant ISCs for predicting EF, LASSO regression with 10-fold cross-validation was implemented. Only the ISCs surviving LASSO's penalty were entered into a final robust linear regression model using the MASS package in R. This approach is less sensitive to outliers and heteroskedasticity, and we further employed heteroskedasticity-consistent standard errors (from the sandwich package) to maintain statistical rigor. In each regression, we controlled for a series of a priori clinical and demographic covariates (e.g., gestational age, high social risk, bronchopulmonary dysplasia), which were all standardized for interpretive clarity. Statistical significance was evaluated at $p < 0.05$, with one asterisk (*) in tables indicating p-values below this threshold. Additional corrections such as the false discovery rate (FDR) were applied where multiple comparisons were performed (e.g., in canonical correlation analyses).

We used consistent neuroimaging acquisition protocols on a single 3 T system. Standardized pipelines (FSL, MRtrix, and the Brain Connectivity Toolbox) were used for preprocessing and graph metric computations, and motion-corrupted scans were excluded through automated and manual quality checks. Relevant R scripts (including those for NMF, LASSO feature selection, and robust regression) are freely available.

Reporting summary

Further information on research design is available in the Nature Portfolio Reporting Summary linked to this article.

Data availability

All relevant data generated or analyzed during this study have been deposited in Figshare (https://doi.org/10.6084/m9.figshare.28369703.v2)[94]. This repository contains comprehensive structural and structural connectivity metrics derived from diffusion MRI and rsMRI, baseline characteristics (clinical and demographic confounder data for each participant), and Minnesota Executive Function Scale (MEFS) outcomes at 3 years corrected age. SC and FC (subsets of top predictive variables selected via LASSO and top variable scores (individual-level data for the highest-contributing structural and functional connectivity metrics).

Code availability

The NMF network components for both functional and structural data for each graph theory metrics types and source code used in this study is publicly accessible on GitHub: https://github.com/abioty/Neuro_Dev_EF_CINEPS

Received: 10 June 2024; Accepted: 14 February 2025;
Published online: 01 March 2025

References

1. Saigal, S. & Doyle, L. W. An overview of mortality and sequelae of preterm birth from infancy to adulthood. *Lancet* **371**, 261–269 (2008).
2. Blencowe, H. et al. Preterm birth-associated neurodevelopmental impairment estimates at regional and global levels for 2010. *Pediatr. Res*. **74**, 17–34 (2013).
3. Aanes, S., Bjuland, K. J., Skranes, J. & Løhaugen, G. C. C. Memory function and hippocampal volumes in preterm born very-low-birth-weight (VLBW) young adults. *Neuroimage* **105**, 76–83 (2015).
4. Daamen, M. et al. Working memory in preterm-born adults: Load-dependent compensatory activity of the posterior default mode network. *Hum. Brain Mapp.* **36**, 1121–1137 (2015).
5. Kelly, C. E. et al. Working memory training and brain structure and function in extremely preterm or extremely low birth weight children. *Hum. Brain Mapp.* **41**, 684–696 (2020).
6. Lawrence, E. J. et al. The neural basis of response inhibition and attention allocation as mediated by gestational age. *Hum. Brain Mapp.* **30**, 1038–1050 (2009).
7. van Houdt, C. A., Oosterlaan, J., van Wassenaer-Leemhuis, A. G., van Kaam, A. H. & Aarnoudse-Moens, C. S. H. Executive function deficits in children born preterm or at low birthweight: a meta-analysis. *Dev. Med. Child Neurol.* **61**, 1015–1024 (2019).
8. Aarnoudse-Moens, C. S. H., Weisglas-Kuperus, N., van Goudoever, J. B. & Oosterlaan, J. Meta-analysis of neurobehavioral outcomes in very preterm and/or very low birth weight children. *Pediatrics* **124**, 717–728 (2009).
9. Sandoval, C. C., Gaspardo, C. M. & Linhares, M. B. M. The impact of preterm birth on the executive functioning of preschool children: a systematic review. *Appl. Neuropsychol. Child* **11**, 873–890 (2022).
10. Anderson, P. J. Neuropsychological outcomes of children born very preterm. *Sem. Fetal Neonatal Med*. **14**, 90–96 (2014).
11. Mulder, H., Pitchford, N. J., Hagger, M. S. & Marlow, N. Development of executive function and attention in preterm children: a systematic review. *Dev. Neuropsychol.* **34**, 393–421 (2009).
12. Nosarti, C. et al. Preterm birth and structural brain alterations in early adulthood. *NeuroImage: Clin.* **6**, 180–191 (2014).
13. Schnider, B. et al. Altered brain metabolism contributes to executive function deficits in school-aged children born very preterm. *Pediatr. Res.* **88**, 739–748 (2020).
14. Skranes, J. et al. White matter abnormalities and executive function in children with very low birth weight. *Neuroreport* **20**, 263–266 (2009).
15. Ajayi-Obe, M., Saeed, N., Cowan, F. M., Rutherford, M. A. & Edwards, A. D. Reduced development of cerebral cortex in extremely preterm infants. *Lancet* **356**, 1162–1163 (2000).
16. Yuan, W. et al. Effects of intraventricular hemorrhage on white matter microstructural changes at term and early developmental outcomes in infants born very preterm. *Neuroradiology* **63**, 1549–1561 (2021).
17. Parikh, N. A. et al. Objectively diagnosed diffuse white matter abnormality at term is an independent predictor of cognitive and language outcomes in infants born very preterm. *J. Pediatr.* **220**, 56–63 (2020).
18. Kline, J. E. et al. Diffuse excessive high signal intensity in the preterm brain on advanced MRI represents widespread neuropathology. *Neuroimage* **264**, 119727 (2022).
19. Parikh, N. A., Pierson, C. R. & Rusin, J. A. Neuropathology associated with diffuse excessive high signal intensity abnormalities on magnetic resonance imaging in very preterm infants. *Pediatr. Neurol.* **65**, 78–85 (2016).
20. Nosarti, C. et al. Grey and white matter distribution in very preterm adolescents mediates neurodevelopmental outcome. *Brain* **131**, 205–217 (2007).
21. Bassi, L. et al. Diffusion tensor imaging in preterm infants with punctate white matter lesions. *Pediatr. Res.* **69**, 561–566 (2011).
22. Murray, A. L. et al. White matter abnormalities and impaired attention abilities in children born very preterm. *Neuroimage* **124**, 75–84 (2016).
23. Giménez, M. et al. White matter volume and concentration reductions in adolescents with history of very preterm birth: a voxel-based morphometry study. *Neuroimage* **32**, 1485–1498 (2006).
24. Degnan, A. J. et al. Altered structural and functional connectivity in late preterm preadolescence: an anatomic seed-based study of resting state networks related to the posteromedial and lateral parietal cortex. *PLoS ONE* **10**, e0130686 (2015).
25. Tseng, C.-E. J. et al. Working memory training is associated with changes in resting state functional connectivity in children who were born extremely preterm: a randomized controlled trial. *J. Cogn. Enhanc.***3**, 376–387 (2019).
26. Caldinelli, C. et al. White matter alterations to cingulum and fornix following very preterm birth and their relationship with cognitive functions. *Neuroimage* **150**, 373–382 (2017).
27. Karolis, V. R. et al. Reinforcement of the brain's rich-club architecture following early neurodevelopmental disruption caused by very preterm birth. *Cereb. Cortex* **26**, 1322–1335 (2016).
28. Schmitz-Koep, B. et al. Grey and white matter volume changes after preterm birth: a meta-analytic approach. *J. Pers. Med.* **11**, 868 (2021).
29. Bjuland, K. J., Løhaugen, G. C. C., Martinussen, M. & Skranes, J. Cortical thickness and cognition in very-low-birth-weight late teenagers. *Early Hum. Dev.* **89**, 371–380 (2013).
30. Kapellou, O. et al. Abnormal cortical development after premature birth shown by altered allometric scaling of brain growth. *PLoS Med.* **3**, e265 (2006).
31. Kline, J. E. et al. Early cortical maturation predicts neurodevelopment in very preterm infants. *Arch. Dis. Child. Fetal Neonatal Ed.* **105**, 460–465 (2020).
32. Dean, J. M. et al. Prenatal cerebral ischemia disrupts MRI-defined cortical microstructure through disturbances in neuronal arborization. *Sci. Transl. Med.* **5**, 168ra167–168ra167 (2013).
33. Lax, I. D. et al. Neuroanatomical consequences of very preterm birth in middle childhood. *Brain Struct. Funct.* **218**, 575–585 (2013).
34. Kline, J. E. et al. Diffuse white matter abnormality in very preterm infants at term reflects reduced brain network efficiency. *NeuroImage Clin.* **31**, 102739 (2021).
35. Volpe, J. J. Brain injury in premature infants: a complex amalgam of destructive and developmental disturbances. *Lancet Neurol.* **8**, 110–124 (2009).
36. Mürner-Lavanchy, I. M. et al. Thirteen-year outcomes in very preterm children associated with diffuse excessive high signal intensity on neonatal magnetic resonance imaging. *J. Pediatr.* **206**, 66–71. e61 (2019).
37. Della Rosa, P. A. et al. The effects of the functional interplay between the Default Mode and Executive Control Resting State Networks on

cognitive outcome in preterm born infants at 6 months of age. *Brain Cogn.* **147**, 105669 (2021).
38. He, L. & Parikh, N. A. Aberrant executive and frontoparietal functional connectivity in very preterm infants with diffuse white matter abnormalities. *Pediatr. Neurol.* **53**, 330–337 (2015).
39. van den Heuvel, M. P. et al. The neonatal connectome during preterm brain development. *Cereb. Cortex* **25**, 3000–3013 (2014).
40. Ball, G. et al. Rich-club organization of the newborn human brain. *Proc. Natl. Acad. Sci.* **111**, 7456–7461 (2014).
41. Doria, V. et al. Emergence of resting state networks in the preterm human brain. *Proc. Natl. Acad. Sci.* **107**, 20015–20020 (2010).
42. Smyser, C. D. et al. Longitudinal analysis of neural network development in preterm infants. *Cereb. Cortex* **20**, 2852–2862 (2010).
43. Smyser, C. D., Wheelock, M. D., Limbrick, D. D. Jr & Neil, J. J. Neonatal brain injury and aberrant connectivity. *Neuroimage* **185**, 609–623 (2019).
44. Burzynska, A. Z. et al. A scaffold for efficiency in the human brain. *J. Neurosci.* **33**, 17150–17159 (2013).
45. Honey, C. J. et al. Predicting human resting-state functional connectivity from structural connectivity. *Proc. Natl. Acad. Sci.* **106**, 2035–2040 (2009).
46. Menon, V. & Uddin, L. Q. Saliency, switching, attention and control: a network model of insula function. *Brain Struct. Funct.* **214**, 655–667 (2010).
47. Corbetta, M. & Shulman, G. L. Control of goal-directed and stimulus-driven attention in the brain. *Nat. Rev. Neurosci.* **3**, 201–215 (2002).
48. Menon, V. Large-scale brain networks and psychopathology: a unifying triple network model. *Trends Cogn. Sci.* **15**, 483–506 (2011).
49. Fair, D. A. et al. The maturing architecture of the brain's default network. *Proc. Natl. Acad. Sci.* **105**, 4028–4032 (2008).
50. Bullmore, E. & Sporns, O. The economy of brain network organization. *Nat. Rev. Neurosci.* **13**, 336–349 (2012).
51. Heuvel, M. P. V. D., Stam, C. J., Kahn, R. S. & Pol, H. E. H. Efficiency of functional brain networks and intellectual performance. *J. Neurosci.* **29**, 7619–7624 (2009).
52. Batalle, D. et al. Early development of structural networks and the impact of prematurity on brain connectivity. *Neuroimage* **149**, 379–392 (2017).
53. Tymofiyeva, O. et al. Towards the "baby connectome": mapping the structural connectivity of the newborn brain. *PLoS ONE* **7**, e31029 (2012).
54. Medaglia, J. D., Lynall, M.-E. & Bassett, D. S. Cognitive network neuroscience. *J. Cogn. Neurosci.* **27**, 1471–1491 (2015).
55. Shine, J. M. et al. The low-dimensional neural architecture of cognitive complexity is related to activity in medial thalamic nuclei. *Neuron* **104**, 849–855.e843 (2019).
56. Basten, U., Hilger, K. & Fiebach, C. J. Where smart brains are different: a quantitative meta-analysis of functional and structural brain imaging studies on intelligence. *Intelligence* **51**, 10–27 (2015).
57. Neubauer, A. C. & Fink, A. Intelligence and neural efficiency. *Neurosci. Biobehav. Rev.* **33**, 1004–1023 (2009).
58. Fischi-Gómez, E. et al. Structural brain connectivity in school-age preterm infants provides evidence for impaired networks relevant for higher order cognitive skills and social cognition. *Cereb. Cortex* **25**, 2793–2805 (2014).
59. Barnes-Davis, M. E., Williamson, B. J., Merhar, S. L., Holland, S. K. & Kadis, D. S. Rewiring the extremely preterm brain: altered structural connectivity relates to language function. *NeuroImage: Clin.* **25**, 102194 (2020).
60. Barnes-Davis, M. E. et al. Structural connectivity at term equivalent age and language in preterm children at 2 years corrected. *Brain Commun.* **6**, fcae126 (2024).
61. Gratton, C., Sun, H. & Petersen, S. E. Control networks and hubs. *Psychophysiology* **55**, e13032 (2018).
62. Crittenden, B. M., Mitchell, D. J. & Duncan, J. Task encoding across the multiple demand cortex is consistent with a frontoparietal and cingulo-opercular dual networks distinction. *J. Neurosci.* **36**, 6147–6155 (2016).
63. Sun, H. et al. Network controllability of structural connectomes in the neonatal brain. *Nat. Commun.* **14**, 5820 (2023).
64. Scheinost, D. et al. Cerebral lateralization is protective in the very prematurely born. *Cereb. Cortex* **25**, 1858–1866 (2015).
65. Roberts, G. et al. Rates of early intervention services in very preterm children with developmental disabilities at age 2 years. *J. Paediatr. Child Health* **44**, 276–280 (2008).
66. Mahabee-Gittens, E. M. et al. Prenatal opioid exposure and risk for adverse brain and motor outcomes in infants born premature. *J. Pediatr.* **267**, 113908 (2024).
67. Parikh, N. A. et al. Perinatal risk and protective factors in the development of diffuse white matter abnormality on term-equivalent age magnetic resonance imaging in infants born very preterm. *J. Pediatr.* **233**, 58–65. e53 (2021).
68. Carlson, S. & Zelazo, P. Minnesota executive function scale: test manual. Reflection Sciences (2014).
69. Zelazo, P. D. The Dimensional Change Card Sort (DCCS): a method of assessing executive function in children. *Nat. Protoc.* **1**, 297–301 (2006).
70. Lee, K., Bull, R. & Ho, R. M. Developmental changes in executive functioning. *Child Dev.* **84**, 1933–1953 (2013).
71. Beck, D. M., Schaefer, C., Pang, K. & Carlson, S. M. Executive function in preschool children: test–retest reliability. *J. Cogn. Dev.* **12**, 169–193 (2011).
72. Meuwissen, A. et al. The psychometrics of the Minnesota Executive Function Scale. Society for Research in Child Development (2017).
73. Carlson, S. & Zelazo, P. Minnesota executive function scale: Technical report. Reflection Sciences (2017).
74. Jenkinson, M., Beckmann, C. F., Behrens, T. E., Woolrich, M. W. & Smith, S. M. Fsl. *Neuroimage* **62**, 782–790 (2012).
75. Jenkinson, M., Bannister, P., Brady, M. & Smith, S. Improved optimization for the robust and accurate linear registration and motion correction of brain images. *Neuroimage* **17**, 825–841 (2002).
76. Andersson, J. L., Jenkinson, M. & Smith, S. Non-linear registration, aka Spatial normalisation FMRIB technical report TR07JA2. *FMRIB Anal. Group Univ. Oxf.* **2**, 1–22 (2007).
77. Paydar, A. et al. Diffusional kurtosis imaging of the developing brain. *Am. J. Neuroradiol.* **35**, 808–814 (2014).
78. Smith, R. E., Tournier, J.-D., Calamante, F. & Connelly, A. The effects of SIFT on the reproducibility and biological accuracy of the structural connectome. *Neuroimage* **104**, 253–265 (2015).
79. Makropoulos, A. et al. Regional growth and at lasing of the developing human brain. *Neuroimage* **125**, 456–478 (2016).
80. Makropoulos, A. et al. Automatic whole brain MRI segmentation of the developing neonatal brain. *IEEE Trans. Med. Imaging* **33**, 1818–1831 (2014).
81. Klein, A. et al. Evaluation of 14 nonlinear deformation algorithms applied to human brain MRI registration. *Neuroimage* **46**, 786–802 (2009).
82. Smith, S. M. et al. Advances in functional and structural MR image analysis and implementation as FSL. *Neuroimage* **23**, S208–S219 (2004).
83. Fitzgibbon, S. P. et al. The developing Human Connectome Project (dHCP) automated resting-state functional processing framework for newborn infants. *Neuroimage* **223**, 117303 (2020).
84. Shi, F., Salzwedel, A. P., Lin, W., Gilmore, J. H. & Gao, W. Functional brain parcellations of the infant brain and the associated developmental trends. *Cereb. Cortex* **28**, 1358–1368 (2018).
85. Whitfield-Gabrieli, S. & Nieto-Castanon, A. Conn: a functional connectivity toolbox for correlated and anticorrelated brain networks. *Brain Connect* **2**, 125–141 (2012).

86. Lee, D. & Seung, H. S. Algorithms for non-negative matrix factorization. *Adv. Neural Inf. Process. Syst.* **13** (2000).
87. Hyvarinen, A. & Oja, E. Independent component analysis: algorithms and applications. *Neural Netw.* **13**, 411–430 (2000).
88. Brunet, J. P., Tamayo, P., Golub, T. R. & Mesirov, J. P. Metagenes and molecular pattern discovery using matrix factorization. *Proc. Natl. Acad. Sci. USA* **101**, 4164–4169 (2004).
89. Boutsidis, C. & Gallopoulos, E. SVD based initialization: a head start for nonnegative matrix factorization. *Pattern Recognit.* **41**, 1350–1362 (2008).
90. Sotiras, A., Resnick, S. M. & Davatzikos, C. Finding imaging patterns of structural covariance via non-negative matrix factorization. *Neuroimage* **108**, 1–16 (2015).
91. Jensen, E. A. et al. The diagnosis of bronchopulmonary dysplasia in very preterm infants. An evidence-based approach. *Am. J. Respir. Crit. Care Med.* **200**, 751–759 (2019).
92. Kidokoro, H., Neil, J. J. & Inder, T. E. New MR imaging assessment tool to define brain abnormalities in very preterm infants at term. *Am. J. Neuroradiol.* **34**, 2208–2214 (2013).
93. Zeileis, A. Object-oriented computation of sandwich estimators. *J. Stat. Softw.* **16**, 1–16 (2006).
94. Derbie, A. Y. et al. Multimodal brain connectivity, baseline characteristics, and executive function in preterm infants. https://doi.org/10.6084/m9.figshare.28369703.v2 (2025).

Acknowledgements

The authors would like to thank the CINEPS investigators and the participating children and families for their dedication to scientific research. This work was funded by awards from the National Institute of Neurological Disorders and Stroke (NINDS) of NIH grants R01-NS094200 and R01-NS096037 to N.A.P. and R01 EB029944-01 from the National Institute of Biomedical Imaging and Bioengineering (NIBIB) to L.H.

Author contributions

Conceptualization: A.Y.D., N.A.P., L.T.; methodology: A.Y.D., N.A.P., M.A., L.H., A.A., J.W.; data analysis: A.Y.D., N.A.P., M.A., J.W.; data acquisition: N.A.P., L.H.; interpretation of results: A.Y.D., N.A.P., W.A., L.T; funding acquisition: N.A.P.; project administration: N.A.P; supervision: N.A.P, M.A.; writing—original draft: A.Y.D., N.A.P.; writing—review & editing: All authors.

Competing interests

The authors declare no competing interests.

Additional information

Supplementary information The online version contains supplementary material available at https://doi.org/10.1038/s42003-025-07745-1.

Correspondence and requests for materials should be addressed to Nehal A. Parikh.

Peer review information *Communications Biology* thanks Vyacheslav Karolis and the other, anonymous, reviewer for their contribution to the peer review of this work. Primary Handling Editor: Benjamin Bessieres. A peer review file is available.

Reprints and permissions information is available at http://www.nature.com/reprints

Publisher's note Springer Nature remains neutral with regard to jurisdictional claims in published maps and institutional affiliations.

Open Access This article is licensed under a Creative Commons Attribution-NonCommercial-NoDerivatives 4.0 International License, which permits any non-commercial use, sharing, distribution and reproduction in any medium or format, as long as you give appropriate credit to the original author(s) and the source, provide a link to the Creative Commons licence, and indicate if you modified the licensed material. You do not have permission under this licence to share adapted material derived from this article or parts of it. The images or other third party material in this article are included in the article's Creative Commons licence, unless indicated otherwise in a credit line to the material. If material is not included in the article's Creative Commons licence and your intended use is not permitted by statutory regulation or exceeds the permitted use, you will need to obtain permission directly from the copyright holder. To view a copy of this licence, visit http://creativecommons.org/licenses/by-nc-nd/4.0/.

© The Author(s) 2025